The pseudo-Voigt function is an approximation to the Voigt function, which is the convolution of a Gaussian and a Lorentzian:

Voigt function

$$P_V(\Delta, \Gamma_L, \Gamma_G) = \int_{-\infty}^{\infty} P_L(\Delta, \Gamma_l) P_G(\Delta - \delta, \Gamma_G)\, \mathrm{d}\delta = \left(\frac{4 \ln 2}{\pi \Gamma_G^2}\right)^{1/2} \mathrm{Re}[\exp(-z^2)\mathrm{erfc}(-iz)], \quad (3.3.9)$$

where $z = \alpha + i\beta$, $\alpha = (4 \ln 2)^{1/2} \Delta/\Gamma_G$ and $\beta = (\ln 2)^{1/2} \Gamma_L/\Gamma_G$.

A number of formulations have been proposed for the pseudo-Voigt coefficients to make the best fit to the corresponding Voigt function (Hastings *et al.*, 1984; David, 1986; Thompson *et al.*, 1987). The latter is most commonly used and gives overall the FWHM, Γ and the mixing coefficient, η, to be used in equation (3.3.8) as functions of the individual FWHMs Γ_G and Γ_L:

$$\Gamma = [(\Gamma_G^5 + 2.69269\Gamma_G^4\Gamma_L + 2.42843\Gamma_G^3\Gamma_L^2 + 4.47163\Gamma_G^2\Gamma_L^3 + 0.07842\Gamma_G\Gamma_L^4 + \Gamma_L^5)]^{1/5}, \quad (3.3.10)$$

$$\eta = 1.36603(\Gamma_L/\Gamma) - 0.47719(\Gamma_L/\Gamma)^2 + 0.11116(\Gamma_L/\Gamma)^3. \quad (3.3.11)$$

The alternative given by David (1986) uses a more generalized version of the pseudo-Voigt function,

$$\begin{aligned} P_{\mathrm{PV}}(\Delta, W_G, W_L, \eta_G, \eta_L) &= \eta_L P_L(\Delta, W_L) + \eta_G P_G(\Delta, W_G), \\ \eta_G &= 0.00268\rho_1 + 0.75458\rho_1^2 + 2.88898\rho_1^3 - 3.85144\rho_1^4 \\ &\quad - 0.55765\rho_1^5 + 3.03824\rho_1^6 - 1.27539\rho_1^7, \\ \eta_L &= 1.35248\rho_2 + 0.41168\rho_2^2 - 2.18731\rho_2^3 + 6.42452\rho_2^4 \\ &\quad - 10.29036\rho_2^5 + 6.88093\rho_2^6 - 1.59194\rho_2^7, \\ W_G &= \Gamma(1 - 0.50734\rho_2 - 0.22744\rho_2^2 + 1.63804\rho_2^3 \\ &\quad - 2.28532\rho_2^4 + 1.31943\rho_2^5), \\ W_L &= \Gamma(1 - 0.99725\rho_1 + 1.14594\rho_1^2 + 2.56150\rho_1^3 \\ &\quad - 6.52088\rho_1^4 + 5.82647\rho_1^5 - 1.91086\rho_1^6), \end{aligned} \quad (3.3.12)$$

where $\Gamma = \Gamma_G + \Gamma_L$, $\rho_1 = \Gamma_G/\Gamma$ and $\rho_2 = \Gamma_L/\Gamma$; this is claimed to match the Voigt function to better than 0.3%.

3.3.2.2. *Constant-wavelength powder profile asymmetry*

Rietveld (1969) noted that at very low scattering angles the peaks displayed some asymmetry, which shifted the peak maximum to lower angles. He ascribed the effect to 'vertical divergence' and proposed a purely empirical correction for it. Subsequent authors (Cooper & Sayer, 1975; Howard, 1982; Hastings *et al.*, 1984) offered semi-empirical treatments of the profile shape that results from the intersection of a Debye–Scherrer cone with a finite receiving slit, which is described as 'axial divergence'. A more complete analysis of the problem in neutron powder diffraction was offered by van Laar & Yelon (1984), who considered the effect of a finite vertical slit ($2H$) intercepting a set of Bragg diffraction cones generated from a finite sample length ($2S$) within the incident beam for a goniometer radius (L). As seen in Fig. 3.3.1, this gives peak intensity beginning at $2\varphi_{\min} < 2\theta$ *via* scattering from only the ends of the sample; at $2\varphi_{\mathrm{infl}}$ the entire sample scatters into the detector. The resulting intensity profile is then convoluted with a Gaussian function to give the resulting asymmetric powder line profile (Fig. 3.3.2). This approach was then considered by Finger *et al.* (1994) for synchrotron powder diffraction and they created a Fortran code that was subsequently adopted *via* convolution with a pseudo-Voigt function [equation (3.3.12)] for use by many Rietveld refinement codes. Although originally formulated for parallel-beam neutron optics, it was shown by Finger *et al.* (1994) that it could be equally well applied to diverging X-ray and neutron optics by allowing the sample length to vary during the Rietveld refinement. They also showed that it could be applied to the asymmetry observed at low angles with Bragg–Brentano instrumentation. In that case the detector height is defined by the diffracted-beam Soller slits.

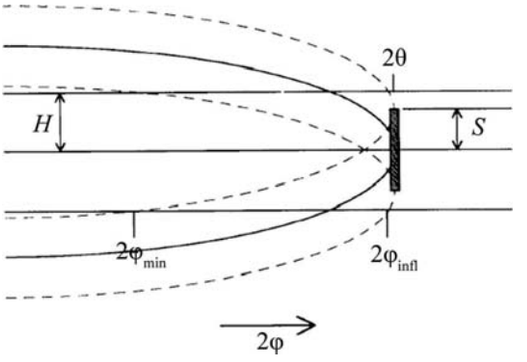

Figure 3.3.1
The band of intensity diffracted by a sample with height $2S$, as seen by a detector with opening $2H$ and a detector angle 2φ moving in the detector cylinder. For angles below $2\varphi_{\min}$ no intensity is seen. For angles between $2\varphi_{\mathrm{infl}}$ and 2θ, scattering from the entire sample can be seen by the detector. Figure and caption adapted from Finger *et al.* (1994).

Clearly, this asymmetric peak-shape function properly represents the offset of the peak top from the peak position, in contrast to functions such as the split Pearson VII function. Consequently, single peak fits using this function will give peak positions that are more readily indexed using methods such as those described in Chapter 3.4.

3.3.2.3. *Peak-displacement effects*

The position of the peak is also affected by various instrumental and geometric effects. For example, the sample position in a Bragg–Brentano experiment is ideally tangent to the focusing circle (Parrish, 1992). A radial displacement, s, of the sample will shift the Bragg peaks according to

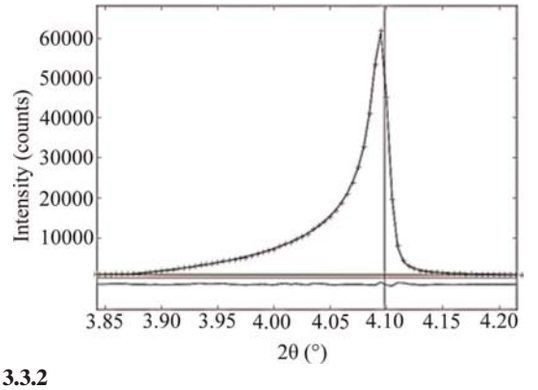

Figure 3.3.2
Low-angle synchrotron powder diffraction line ($2\theta \simeq 4.1^\circ$) fitted by the Finger *et al.* (1994) axial divergence powder line-shape function. The observed points (+), calculated curve, background and difference curves are shown. Note the offset of the peak top from the Bragg 2θ position (vertical line).